Cleaning and recirculation of perfluorohexane (C_6F_{14}) in the STAR-RICH detector

Y. Andres[a], A. Braem[a], D. Cozza[b], M. Davenport[a], G. De Cataldo[b],
L. Dell Olio[b], D. DiBari[b], A. DiMauro[a], J.C. Dunlop[c], E. Finch[d],
D. Fraissard[a], A. Franco[b], J. Gans[c], B. Ghidini[b], J.W. Harris[c], M. Horsley[c],
G.J. Kunde[c], B. Lasiuk[c,*], Y. Lesenechal[a], R.D. Majka[d], P. Martinengo[a],
A. Morsch[a], E. Nappi[b], G. Paic[a], F. Piuz[a], F. Posa[b], J. Raynaud[a], S. Salur[c],
J. Sandweiss[d], J.C. Santiard[a], J. Satinover[c], E. Schyns[a], N. Smirnov[c],
J. Van Beelen[a], T.D. Williams[a], Z. Xu[d]

[a] *CERN HMPID Group, CERN, Geneva CH-1211, Switzerland*
[b] *Bari HMPID Group, Bari, Sez. INFN and Dipartimento di Fisica, Bari 70124, Italy*
[c] *Physics Department, Yale University, Yale RHI Group, P.O. Box 208124, New Haven, CT 06520-8124, USA*
[d] *Yale HE Group, New Haven, CT 06520, USA*

The STAR-RICH collaboration[1]

Received 22 August 2001; accepted 29 October 2001

Abstract

A RICH detector with a CsI photo-cathode and liquid perfluorohexane radiator has been installed in the STAR experiment at RHIC. The liquid is continuously cleaned and distributed to a quartz containment vessel within the detector by a closed recirculation system. A VUV spectrometer is connected to the system which monitors the optical transparency of the liquid. This measurement provides one of the pieces of information necessary to model the number of Cherenkov photons which reach the pad plane. A description of the liquid recirculation system and the cleaning procedure for the liquid as well as the spectrometer is presented along with results of their performance. © 2001 Elsevier Science B.V. All rights reserved.

1. Introduction

The use of thin-film CsI for photo-cathodes in Ring Imaging Cherenkov (RICH) detectors is becoming more wide spread [1–3]. This technology has been chosen for the RICH in the ALICE heavy ion experiment [1]. The ALICE RICH is designed to provide particle identification in the momentum region between 1 and 5 GeV/c. A conceptual drawing of the $\frac{2}{3}$ size prototype module components of the ALICE detector, developed at CERN, is shown in Fig. 1. It is described in detail elsewhere [4]. It is this detector which has been installed in the STAR detector at BNL [5].

*Corresponding author.
E-mail address: brian.lasiuk@yale.edu (B. Lasiuk).
[1] Bari/CERN ALICE-HMPID groups and Yale.

This detector utilizes a 300 nm film of CsI, deposited on a segmented cathode pad plane, as a photo-converter. CsI has a photo-electric threshold of 6.0 eV which restricts its sensitivity to photons in the Vacuum Ultra-Violet (VUV) region. The quantum efficiency of CsI for the STAR-RICH photo cathodes is shown in the left panel of Fig. 2. This spectral sensitivity imposes restrictions on the materials used in the construction and operation of the detector, and most

importantly on the optical properties of the radiator. In order to extend particle identification capabilities beyond a momentum of 1.5 GeV/c, the radiator must possess an appropriate index of refraction (i.e. $\leqslant 1.30$) and transmit photons in the VUV region of the spectrum. The perfluoroalkanes are some of the few substances which are transparent to radiation in this region and perfluorohexane (C_6F_{14}) is suitable for the momentum region of interest with an index of refraction of 1.29 at 190 nm [7] as seen in the right panel of Fig. 2.
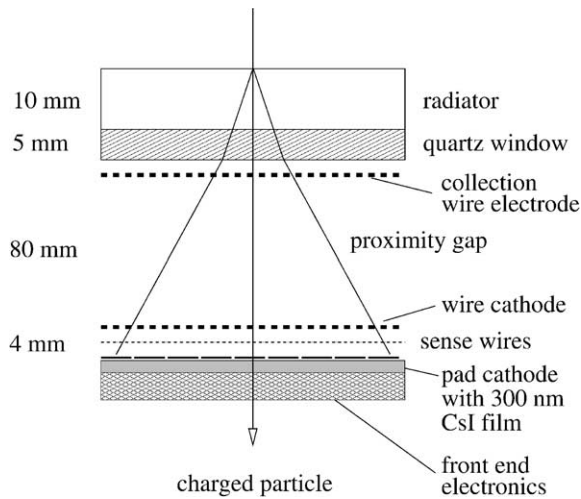
2. Liquid radiator

Perfluorohexane is a dense colorless, odorless, liquid at Standard Temperature and Pressure (STP). It is quite volatile but non-toxic and chemically inert. It has a great capacity for dissolving gases and although hydrophobic, it will dissolve water at the ppm level. Some basic properties of perfluorohexane are shown in Table 1. It is available in many grades and purities, but in no case is care taken to isolate it from either water or oxygen, both common substances which strongly absorb UV radiation. In consideration of cost and past experience from other RICH detectors [8], a solvent grade of this liquid, PF5060-DL, from 3M Chemicals [9] was chosen.

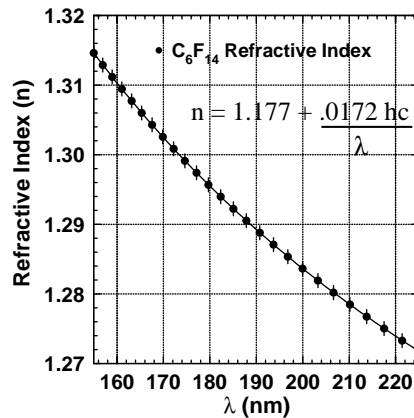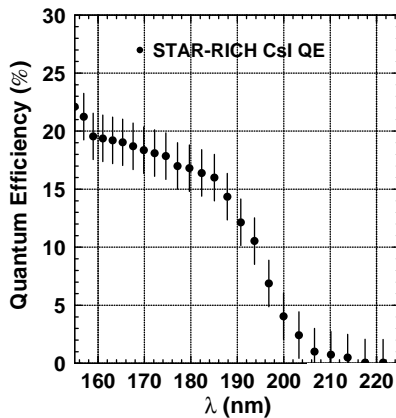Fig. 1. A conceptual drawing of the STAR-RICH detector components.

Fig. 2. The left panel shows the quantum efficiency of the CsI photo cathodes used in the STAR-RICH detector with error bars of $\pm 2\%$ on each point. The right panel shows an estimate for the index of refraction of liquid C_6F_{14} with error bars that correspond to an uncertainty of 1×10^{-3} [6].

Table 1
Selected properties of commercial grade perfluorohexane used in the STAR-RICH detector. Values are given at a temperature of 25°C

Physical properties of perfluorohexane	
Molecular weight (amu)	338
Vapor pressure (mbar)	309
Refractive index at $\lambda = 190$ nm	1.29
Specific gravity	1.68
H_2O solubility (ppm by weight)	10
Air solubility (ml gas/100 ml liquid)	48
O_2 solubility (ml gas/100 ml liquid)	65

3. Liquid recirculation system

The liquid recirculation system for the STAR-RICH detector continuously purifies and distributes fluid to the radiator vessels of the detector. In order to do this safely, it is divided into two parts—a circulation and a distribution rack. A schematic of the system is shown in Fig. 3. The circulation rack contains the main liquid reservoir which has a capacity of 100 l as well as the system pump, filtration system, and vapor recovery refrigerator. The cover gas volume in the main reservoir is connected to the distribution rack by a 3/4 in. (ϕ) siphon-free aerial line. Dry nitrogen flows into the system at a rate of $\sim 15 \, \text{l h}^{-1}$. This isolates the liquid from the atmosphere, provides a means to carry away impurities which out-gas from the liquid, and allows regulation of the relative system pressure. The water content in the exhaust vapor is measured to be $\leqslant 3$ ppm under nominal conditions. A positive 2 mbar over pressure is maintained by the exhaust oil bubbler (OB) upstream of a cold trap (CT). Propylene glycol at $-25°C$, is circulated in the cold trap which condenses the volatile C_6F_{14} vapor from the exhaust gas stream. This reduces the liquid loss by $\sim 75\%$ as compared to the expectation with no cold trap.

The liquid is continuously circulated by a magnetic impeller pump at a pressure of 1.5 bar through cleaning filters (F1). The filters are described in more detail in Section 3.1. Flow-meters regulate the liquid flow to the 4 l header columns (H1) in the distribution rack to $6 \, \text{l h}^{-1}$. The header columns in turn feed liquid into the 5 l radiator vessels under gravity flow. The header tubes decouple the radiator vessels from the pump in the circulation rack and trap gas bubbles in the input streams before they can enter the radiators. The finite volume serves to buffer the liquid volume which maintains a constant flow through the radiators even under small variations in pump output. The columns are situated at a fixed relative height with respect to the radiator vessels inside the detector. This ensures the maximum hydrostatic pressure of the liquid in the column, and therefore on the radiator vessels, does not exceed 85 mbar. Under normal operating conditions when the radiators are full, the 20 cm head of liquid in the columns produce a hydrostatic pressure of 35 mbar which generates a flow of $3 \, \text{l h}^{-1}$ through the throttling valve (V2). The excess flow to the header columns falls into the overflow tank. The liquid flow enters the radiator vessel from the bottom when pneumatic valve V1 is closed. Once filled, the radiators overflow at the top, and the liquid is returned to the over-flow tank in the distribution rack, and subsequently to the main reservoir in the circulation rack, all under gravity flow. In order to ensure safe operation, the drain valve V1 is open when unpowered. As such the radiator will drain to avoid possible over pressurization should the power fail. A sample cell (SC) is connected to the system which allows an in situ measurement of the liquid transparency. The details of this device are contained in Section 4.

A SIEMENS Programmable Logic Controller (PLC S7-300) continuously monitors the operation of the system. The PLC is controlled and read-out through a BridgeView (v2.0) interface running on a PC. Pressures and temperatures of the fluid are measured at critical points in the system and stored in a data base. Software interlocks are implemented to ensure that pressures exerted on the quartz radiator vessels do not exceed the hydrostatic pressure applied by the filled columns. The inherent passive safety of a gravity feed system means that almost any abnormal pressurization can be mitigated by allowing the radiators to drain (open valve V1) and stopping the flow of liquid (i.e. the pump) to the header columns.

In order to avoid chronic degradation of materials due to long-term exposure to
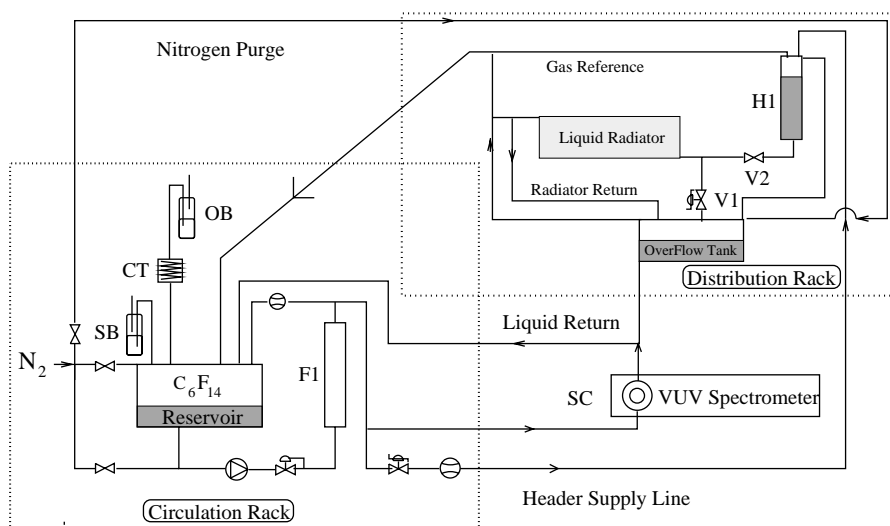
Fig. 3. A schematic of the two racks, each outlined by the dotted squares, which comprise the liquid recirculation system. The circulation rack is responsible for filtration and vapor recovery while the distribution rack delivers liquid to the radiator vessels under gravity flow. Only one header column and one radiator of two is shown for simplicity. The spectrometer is detailed in Section 4. The acronyms are defined in the main text.

perfluorohexane, the wetted parts of the circuit are metal where possible. Stainless steel (SS-316) was used for the valves, mechanical filters, and tubing, as well as the construction of the fluid reservoirs. Aluminum UHV seals connect vacuum flanges where large bore tubing (i.e. > 12 mm) is required. In locations where periodic service is necessary Viton elastomer seals are used. Welded connections or metal pressure fitting are utilized instead of chemical sealants to avoid leaching of compounds into the liquid and glass flow-meters/indicators are used instead of plastic.

In order to ensure the cleanliness of the tubing and components for the recirculation system, two cleaning processes were used. The inside surfaces of the SS elements of the system racks were cleaned following the *Net Inox* process.[2] The elements were degreased with a mild detergent in an ultra-sonic bath at a temperature of 50°C for 60 min. They were then rinsed with water before being immersed in an acid bath for 60 min. After a rinse with demineralized water, the acid residue was neutralized in another detergent bath for

---

[2] The CERN ST/SM-CE group has developed this process.

10 min. Finally, the elements were rinsed with distilled water, dried with a clean compressed air jet, then baked in a ventilated oven at 80°C. The SS tubing which connects the two racks and feeds the detector were treated differently. They were cleaned with acetone and rinsed with spectroscopic grade ethyl alcohol. They were then evacuated, and heated to 75°C in an oven for a period of 24 h before being filled with dry nitrogen and capped with SS pressure fittings. Before installation into the circuit, they were rinsed with C_6F_{14}.

3.1. Filtration and cleaning

The C_6F_{14} liquid is dehydrated by exposing it to an activated molecular sieve. This process also removes hydrocarbons and lipid contaminants effectively. Oxygen removal is facilitated through out-gassing into the N_2 atmosphere and subsequent exhaust of the cover gas. In the STAR-RICH application, the liquid goes through a pre-cleaning process which is described in Section 3.2.

The filter/cleaning cartridge in the circulation rack is a stainless-steel cylinder with a diameter of 76 mm (ϕ) and a length of 850 mm. It is packed

with Uetikon 2-mm type 13X molecular sieve pellets [10]. The inlet and exhaust ports of the cartridge contain a 25 μm sintered bronze mesh in order to confine the sieve material to the cartridge volume. After passage through the molecular sieve cartridge, the fluid traverses a large area stainless-steel mechanical filter with 1 μm pores [11] in order to remove dust generated from punch through. A pressure drop of 500 mbar is measured across the filters at a flow rate of $30 \, l \, h^{-1}$.

Molecular sieves absorbents, or zeolites, are highly porous crystalline molecular matrices which contain alkali metals. They possess well-defined pore sizes and a very high surface area per package volume. Their filtration capabilities come from two distinct processes. Molecules can be mechanically trapped in the pore spacings of the matrix, which in the case of size 13X sieve is ~ 10 Å. This provides an efficient means for the removal of large straight chain paraffins and lipid molecules. However, since water has a molecular dimension of ~ 3.4 Å it is not effectively removed by this process. Rather, the electro-positive alkali metals in the sieve material extract polar molecules, such as water, from solution by the formation of van der Waals complexes. The Uetikon 13X sieve is a sodium alumino-silicate[3] which has an equilibrium water capacity of 29% water by weight. For the filter cartridge described above, this corresponds to a capacity of 830 ml of water.

The molecular sieve is received from the manufacturer in bulk with a maximal water content of 1.5% by weight (43 ml/filter cartridge volume) and must be activated prior to installation into the circulation rack. This is done by packing the sieve material into a filter cartridge and heating it to $+200°C$ while flowing anhydrous Ar through the filter cartridge at a rate of $1 \, l \, min^{-1}$ at a pressure of 1 bar. This is done for a period of 24 h at which time the heat is removed, and the exhaust port of the cartridge is closed. The cartridge is allowed to pressurize to 1 bar by the Ar supply, as the system cools. This minimizes diffusion of air into the cartridge. At this point it is ready for insertion into the liquid recirculation system.

---
[3] $5Na_2$–$Al_2O_3 \cdot 14SiO_2 \cdot XH_2O$.

Upon contact with the liquid, the temperature of the sieve cartridge rises to $\sim 55°C$. This is attributable to the heat of wetting of the sieve material. The pressurized Ar that is expelled from the sieve cartridge is exhausted from the recirculation system by a check-valve immediately down stream from the filters and does not come into contact with the fluid in the reservoir. The elevated temperature persists for no more than 10–15 min and returns to normal room temperature.

Although the molecular matrix of the material is supposed to retain its structure, it is used only once and discarded following the procedure established in the DELPHI-RICH [12]. This is done in order to avoid heating molecular sieve material impregnated with C_6F_{14} because non-saturated fluorocarbons, which are more chemically aggressive than saturated compounds, may be generated. Such compounds can have a detrimental effect on the VUV transparency or induce further chemical activity which can affect the optical properties of the liquid. There is also evidence that the attapulgite clay binder does break down in this particular environment. Traces of sub-micron particulates inside the pipe work have been identified by electron microscopy as originating from the molecular sieve [13].

The liquid recirculation system has provisions for other filtration methods. Oxisorb [14] and activated copper have both been utilized in tests at other installations. This has not yet been employed at BNL since both are chemically active and does carry some risk since non-fully fluorinated compounds may undergo chemical reaction [15]. The chemistry of possible reactions with these materials as well as the possible effects on the VUV optical transmission are subjects of ongoing investigations.

3.2. Pre-cleaning

As mentioned in Section 3.1 the liquid is pre-cleaned by a small dedicated cleaning recirculation system before transfer into the main control rack at BNL. This is necessary since the RHIC collider operates continuously for several months per year and the circulation system cannot be taken off-line to clean a new lot of liquid. Fluid is pumped from

a 40 l stainless steel reservoir at a rate of $90 \, l \, h^{-1}$ through a molecular sieve cartridge, as described in Section 3.1. The liquid then passes through a $0.5 \, \mu m$ stainless-steel sintered filter to remove dust generated by the sieve material. Unlike the liquid circulation rack, cleaning is done under a stagnant N_2 atmosphere pressurized to 300–600 mbar in order to keep fluid loss to a minimum. This means that the continuous outgassing of oxygen to the cover gas is reduced as compared to the continually flushed recirculation system. The liquid circulates in the cleaning rack for ~ 1 month prior to its introduction into the detector liquid system. The performance of the pre-cleaning is described in Section 5.2.

3.3. Liquid transparency

The capabilities of a RICH detector are determined by the precision with which the Cherenkov angle can be reconstructed, and this is in turn a function of the number of Cherenkov photons which are detected. The number of photons ultimately observed are governed by several factors.

The yield of Cherenkov photons produced by a relativistic particle in a 10 mm thickness of C_6F_{14} is approximately $6 \, nm^{-1}$ at 190 nm. This yield decreases as λ^{-2} per unit wavelength interval (i.e. $dN/dx \propto d\lambda/\lambda^2$). A fraction of these photons are absorbed by materials within the detector such as the radiator medium, quartz confinement vessel, the gas of the MWPC, etc. The largest loss of photons is due to the absorption of the quartz vessel and the liquid radiator itself. Of the photons which arrive at the pad plane, a fraction fixed by the QE of the CsI film, undergo photo-conversion. The number ultimately observed is determined by the single-electron detection efficiency of the wire chamber. The wavelength dependence on the yield of photo-electrons is shown in Fig. 4. Accounting for the material absorption and CsI quantum efficiency, the effective spectral sensitivity of the detector is between $165 < \lambda(nm) < 200$. The mean (most probable) wavelength of the photons which are converted to photo-electrons is 182.7 nm (176 nm) and the total number of photons expected for a saturated ring is approximately
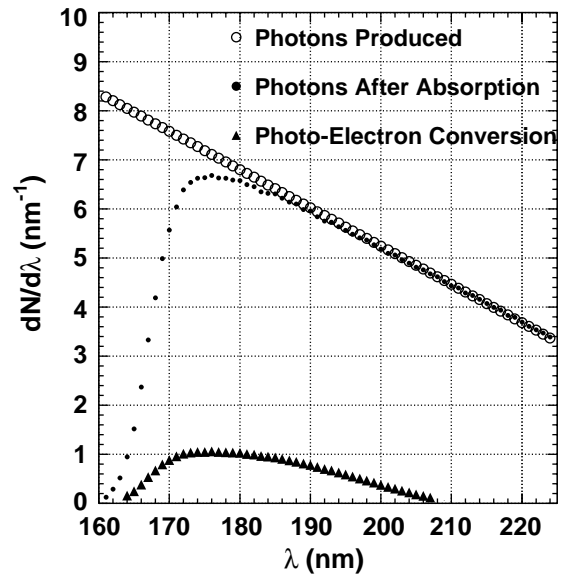

Fig. 4. The wavelength dependence of the yield of Cherenkov photons per nanometer produced in a 10 mm path of perfluorohexane is shown by the open circles. The photon spectrum is attenuated by the finite transmission of the quartz and perfluorohexane[4] as shown by the solid circles. When folded with the quantum efficiency of the CsI (see Fig. 2) the total number of photons, or more precisely, the number of photo-electrons produced in the detector is obtained, illustrated by the solid triangles.

5% of the total generated which corresponds to ~ 12–16. The number of photo-electrons produced is determined by a product of the CsI QE and the liquid transmission; that is, a degradation in either will decrease the number of Cherenkov photons reconstructed. In order to separate the effects of the absorption of the photons in the radiator material from the QE of the CsI on the observed signal, the VUV transparency of the liquid must be measured over the spectral range of the detector.

3.3.1. Contaminants

The purity of 3M PF5060DL is specified to be $\geqslant 90\%$, however, its contaminants are not individually identified, nor is the UV transmission quantified. The proprietary filtration processes to which 3M subjects the liquid eliminates the

---
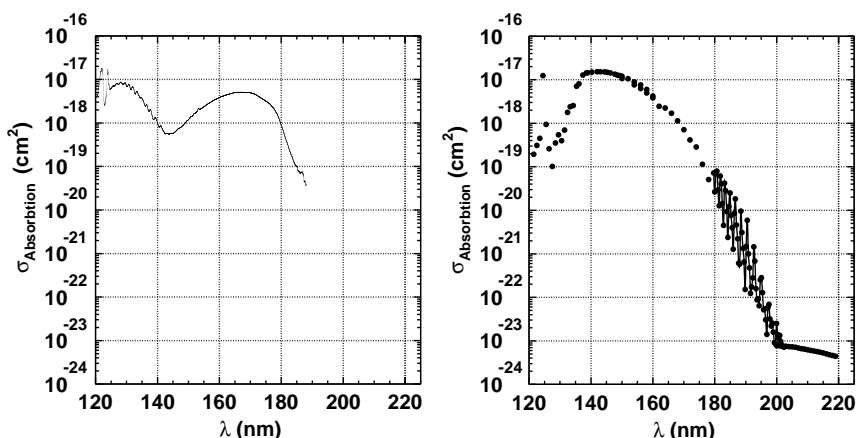
[4]Values published in: Ref. [16].

Fig. 5. The absorption cross-sections for the most important contaminants—water (left) and oxygen (right) are shown here. The data are taken from [17].

presence of cyclic ethers but it is not a priori expected to be free of other organic contaminants.[5] Due to processes in the manufacture of C_6F_{14}, the most probable chemical impurities are similar size fluorocarbons (i.e. pentane, heptane, and octane) and like all synthesized organic compounds, isomer purity is not high. The liquid is packed in a sealed steel drum in contact with air and since C_6F_{14} can dissolve both oxygen and water, they must be reduced to trace quantities before it is suitable for use in our application.

Water and oxygen are important contaminants in the spectral region between $160 < \lambda(\text{nm}) < 220$. These impurities can be present in the raw liquid and are continually outgassing from the detector materials, as well as the pipes that feed liquid to the radiator vessels. The detailed absorption characteristics of both these substances are shown in Fig. 5.

Water strongly absorbs radiation in a continuum between 145 and 185 nm, with a maximum at 166 nm. Below 145 nm a diffuse band structure is observed, however this is in a region well below the cut-off expected from the quartz window and is therefore not important in our application. Molecular oxygen has a broad dissociation continuum

associated with the Schumman–Runge (SR) system over the wavelength range 130–175 nm. Beyond this from 175 to 203 nm the SR band structure, which corresponds to rotational and vibrational excitations of the ground state [18], evolves into the weak Hertzberg continuum. It is noteworthy that only non-dissociate processes occur above 242 nm.

Other contaminants such as hydro-carbons, alcohols, unsaturated fluoro-carbons, ethers and cyclic compounds can also be contained in the liquid and have adverse effects on the VUV transmission. Pure perfluorohexane has been observed to exhibit finite transmission down to a wavelength of 152 nm [19]. Shorter chain saturated fluoro-alkanes do not adversely impact the transparency above this value and the volatility of these compounds means that their long-term presence in the liquid is not an issue. Longer chain perfluorocarbons increase the cut-off wavelength by roughly 10 nm per additional difluoromethylene unit. This is in contrast to the normal hydrocarbon paraffins where the transmission cut-off saturates near 155 nm, independent of the chain length [7]. As such a small component of perfluoroheptane and/or octane can degrade the transmission properties at short wavelengths. A sample of the liquid used in the RICH detector was subjected to a gas chromatography analysis which indicated that composition of the liquid is consistent with heptane and octane at the several

---

[5] 3M supplies various solvent grades of perfluorohexane which differ mainly in the number of distillation and filtration processes.

percent level. Further analysis using infrared spectrometry (i.e. FT-IR) in the wavelength region between 3.0 and 3.6 μm has shown no evidence for alkenes, hydro-carbons, or alcohols in the liquid [20] and recent Nuclear Magnetic Resonance (NMR) measurements have confirmed this [21].

4. The VUV spectrometer

The basic principle of a transparency measurement is to direct a beam of monochromatic light onto a sample of known thickness and measure the ratio of light transmitted through the sample with respect to the total amount of light available. In order to make a precise and reproducible measurement, a method to eliminate or quantify time-dependent variations in the apparatus is required. Such effects include variations in the light source intensity, degradation of the transmission or reflection properties of optical components, drifts in the gain or response of the photo-detectors, as well as dependencies on the absolute calibrations of the instrument. Since the VUV spectrum can be attenutated by atmospheric gases (i.e. oxygen), it is necessary to perform these transmission measurements under vacuum conditions of $\leqslant 10^{-4}$ Torr.

4.1. The spectrometer

A schematic of the VUV spectrometer is shown in Fig. 6. It consists of four modular sections each constructed as a vacuum chamber. They include a (i) light source, (ii) monochromator, (iii) collimation and beam delivery optics, and (iv) photo-detectors.

The light source is a 30 W deuterium discharge lamp (MacPherson model 632) which provides a broadband UV spectrum from 115 to 370 nm. A black-body like spectrum is radiated from 165 to 370 nm while molecular lines dominate the spectral region below. A MgF_2 window is used on the lamp in order to access to the radiation below 165 nm. It defines a 1 mm exit aperture with F/7. MgF_2 is suitable for this application because of its optical and mechanical properties. It allows transmission down to 115 nm and although it is somewhat susceptible to thermal and mechanical shock, it does withstand radiation darkening. It is also one of the least hygroscopic VUV transparent materials. Since the light is generated and transported inside a vacuum chamber, no ozone is produced during the operation of the lamp when the system is evacuated.

The light is focused by a reflective mirror onto adjustable slits which define the entrance aperture
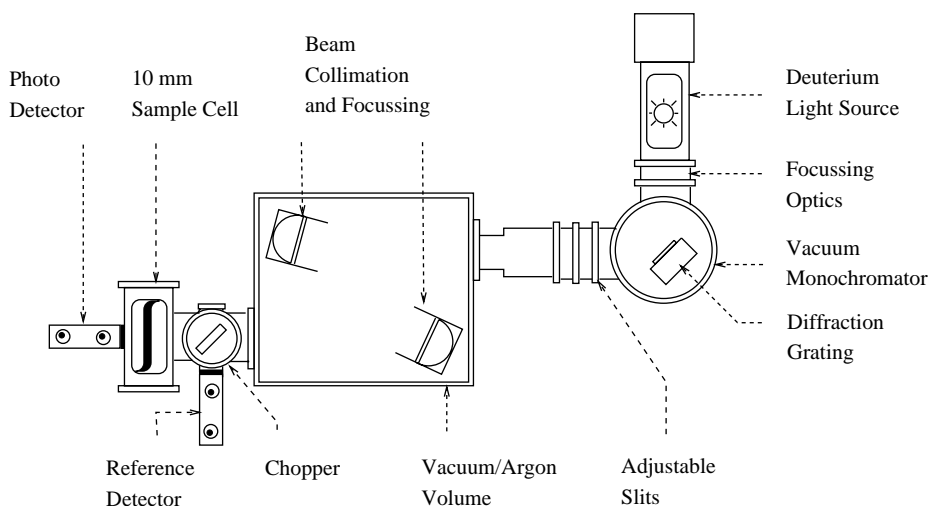

Fig. 6. A schematic of the VUV photo-spectrometer.

of a monochromator (MacPherson model 302). The mirror matches the apertures of the monochromator and light source to reduce the amount of stray light in the system and increase the amount of light delivered to the sample cell. A concave aberration corrected holographic diffraction grating with a rule of $1200 \, mm^{-1}$ is mounted on a rotatable stage within the monochromator housing. A rotation of the stage selects the central wavelength which can be done either manually or under computer control via a RS-232 serial interface. The bandwidth and total flux of the light delivered to the collimation optics is controlled with the input and output slits on the monochromator. They are adjustable by micrometer movements with a $10 \, \mu m$ granularity. In conjunction with the grating, a dispersion of $3.4 \, nm/mm$ is realized and a resolution of $\leqslant 1 \, nm$ is achieved.

The divergent light that emerges from the monochromator is collected and collimated before it is delivered to the sample cell. This is done with one spherical and one off-axis parabolic reflecting first surface mirrors. This was chosen instead of focusing optics for several reasons. First the indices of refraction of materials suitable for lenses in the VUV region (i.e., MgF_2, CaF_2) are strongly wavelength dependent. Therefore, a fixed position lens is not suitable for collimation over a broadband of wavelengths and adaptive optics would have to compensate for these changes. This is expensive and introduces additional systematic uncertainties. Conversely, the focal length of reflective optics is defined purely by the geometric curvature of the surface. Furthermore, degradation due to radiation darkening is eliminated with reflective optics. The beam spot delivered at the output of the collimation chamber to the sample cell from this system is $10 \, mm \, (\phi)$ and has a divergence $< 1 \, mrad$.

The spectrometer has two fixed position photo-detectors—one downstream of the sample cell and one at $90°$ to the beam path which allows a measurement of the total beam power. Two different types of photo-tubes are available. The first are standard Hamamatsu R6095 bi-alkali photo-cathode photo-multiplier tubes (PMT). The entrance windows are coated with $1–2 \, mg \, cm^{-2}$ of sodium salicylate which has a nearly constant QE of 60% over the interval of $90 < \lambda(nm) < 350$. This material emits blue luminescence peaking at a wavelength of 420 nm which matches the bi-alkali PMT peak sensitivity very well. The second set are Hamamatsu R6835 PMTs with CsI photo-cathodes. These are sensitive over a range of 115–200 nm with the peak at 140 nm. As such they are insensitive to any fluorescence at $\lambda > 200 \, nm$ that is radiated from the sample under investigation.

A four-bladed aluminum rotor coated with MgF_2 is mounted at a $45°$ angle to the incident beam downstream of the collimation chamber. When rotating, it alternately allows light to pass either through the sample cell and into the signal detector, or into the reference detector that measures the total beam power. Full transmission/reflection into the arms of the spectrometer maximizes the signal in the photo-detectors and avoids any dependence on the transmission properties of a beam-splitter. Normalizing the output of the signal detector with the reference detector removes time-dependent variations of the lamp intensity, and increases the stability of the measurement. The chopper is driven by a continuously adjustable electric motor at a frequency (v) of 0–400 Hz. A frequency of 90 Hz is used for data taking. A photo-transistor mounted inside the housing senses the position of the rotor and gives a TTL-high-level signal when the light is transmitted through to the sample cell and TTL-low when the light is directed into the reference detector. A second photo-transistor produces a pulse every $v/4$ with a fixed width of $310 \, \mu s$. These signals allow the system to be triggered in two modes; either on every blade, *or* on a specific single blade so that variations in blade reflectivities can be isolated. It is found that the reflectivity coefficients of the different blades vary by as much as 10%, so the system is triggered in single blade mode for the liquid transparency measurements.

The sample under investigation is held in a chamber which can be configured to hold either a mounting stage for solid samples or a cylindrical flow cell for liquid or gas samples. Two flow cells with optical path lengths of 10 and 18 mm are

available. Both have 4 mm MgF_2 windows on the entrance and exit apetures. In this note only results from measurements using the 10 mm cell is reported.

The PMT anode photo-currents are typically 20–60 nA over the spectral range of $165 < \lambda$ (nm) < 225. These currents are converted to voltage signals by high sensitivity linear inverting amplifiers with a conversion of 100 mV nA^{-1}. These amplifiers are based on the Analog Devices AD515A FET op-amp and are mounted directly on the anode of the PMT to minimize the problems associated with transporting a high impedance signal. However, these amplifiers are not suitable for extending the transparency measurements in a continuous fashion below 165 nm because of the intense spectral lines of the deuterium lamp. As such, electronics with a larger dynamic range are necessary to handle the large variation in photo-currents, which reach 5000 nA at 160 nm. Logarithmic amplifiers based on the Burr–Brown 4127 KG were fabricated to cope with this problem.

The data acquisition is controlled by a laptop PC running LabView (v5.0.1). The computer controls all aspects of the acquisition including the scan drive of the monochromator which is operated via the serial port. The two PMT channels are read out with a digitally triggered PCMCIA card, independent of the amplifiers used. The National Instruments DAQ-Card 1200 is capable of sampling 8 analog channels with a 12 bit resolution at a rate of 100 kHz. The strobe signal from the optical chopper is used as a trigger and the signal and reference PMTs are read out sequentially depending on the state of the trigger signal. For each wavelength setting, 1200 measurements of the output photo-current of the PMTs are taken. The mean and width (σ) of these distributions are recorded for off-line analysis.

4.2. The measurement

The spectrometer is configured to measure the relative transmission of a sample in order to reduce the dependencies on the absolute responses and calibrations of the spectrometer components. The relative transmission is a quotient of two separate measurements. In the case of a liquid measurement,

a flow cell is mounted in the sample chamber and a ratio of the total light power transmitted through the liquid filled cell to the total light power transmitted through a control sample, such as N_2, in the same cell, constitutes the measurement.

The first half of the measurement consists of measuring the ratio of the amount of light transmitted through the liquid filled flow cell to the total beam power. In order to avoid the possible build up of contaminants in the cell during the measurement, the liquid flows through the cell at a rate of $\sim 4 \, l \, h^{-1}$. This corresponds to approximately 1 volume change in the flow cell cavity per second. It should be noted that while not in use, a continuous N_2 flow of $6–8 \, l \, h^{-1}$ circulates through the flow cell in order to keep it dry. The spectrometer measures a quantity R_F as a function of wavelength given by

$$R_F(\lambda) = \frac{\Phi \cdot T_F \cdot (R_1 \cdot G_1)_{PMT} \cdot (G_1)_{amp} \cdot (C_1)_{ADC}}{\Phi \cdot R \cdot (R_2 \cdot G_2)_{PMT} \cdot (G_2)_{amp} \cdot (C_2)_{ADC}}$$ (1)

where Φ is the total light flux at the given wavelength, T_F is the transmission of the light through the sample cell when filled with liquid, $(R_{1(2)}G_{1(2)})_{PMT}$ is the response and gain of phototube 1 (2), $(G_{1(2)})_{amp}$ is the gain/conversion of amplifier 1 (2), $(C_{1(2)})_{ADC}$ is the conversion of ADC 1 (2), and R is the reflection coefficient of the chopper blade which directs light into the reference PMT. The wavelength dependence of this ratio is shown in the left panel of Fig. 7. The curve shows features of the spectral shape of the reflectivity of the chopper blades as well asymmetries in the gain and response of the PMTs and the electronics. In order to remove these dependencies, R_F is normalized by a similar measurement which is made with a material of known transparency. For our application, the cell is drained of liquid and flushed with N_2 at a rate of $20 \, l \, h^{-1}$ for five minutes in order to eliminate all liquid and vapors from the cell. The N_2 flow is then reduced to $10 \, l \, h^{-1}$ and a second measurement, R_G, is made:

$$R_G(\lambda) = \frac{\Phi \cdot T_N \cdot (R_1 \cdot G_1)_{PMT} \cdot (G_1)_{amp} \cdot (C_1)_{ADC}}{\Phi \cdot R \cdot (R_2 \cdot G_2)_{PMT} \cdot (G_2)_{amp} \cdot (C_2)_{ADC}}$$ (2)
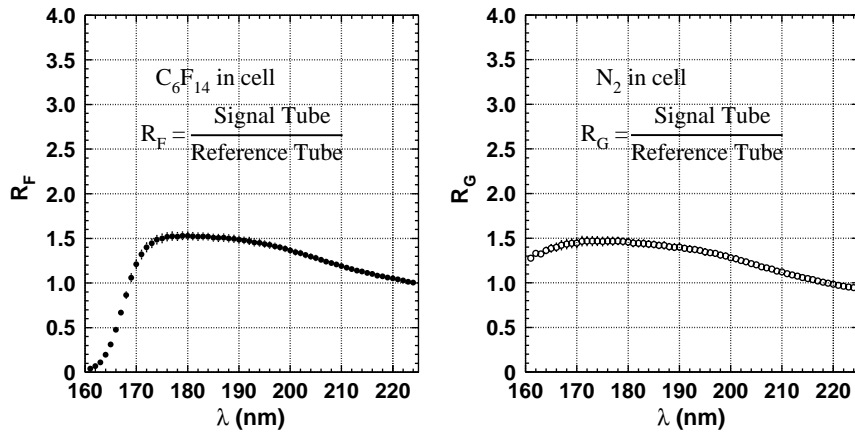
Fig. 7. The ratio R_F, as defined in Eq. (1), is shown in the left panel while the ratio R_G, as shown in Eq. (2) is shown in the right panel. For the C_6F_{14} measurement the flow rate through the sample cell is $4\,1\,h^{-1}$, while it is $10\,1\,h^{-1}$ for the N_2 measurement.
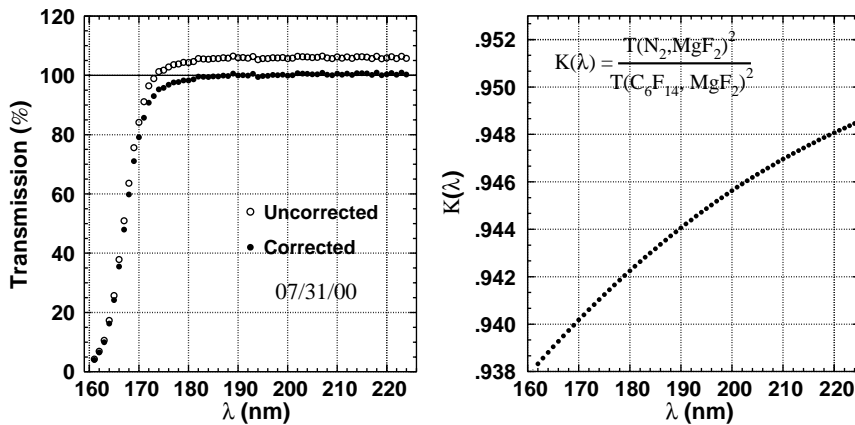

Fig. 8. The transmission for perfluorohexane before and after the correction for Fresnel reflections is shown in the left panel. The correction factor κ which is applied to the super-ratio to determine the corrected transmission is shown in the right panel.

where T_N is the transmission of the light through the sample cell when filled with gas (N_2) and the other quantities are as defined in Eq. (1). The result of such a measurement is shown in the right panel of Fig. 7. Normalizing these two ratios into a super-ratio ($\mathcal{R} = R_F/R_G$) gives the transparency of perfluorohexane relative to N_2. This is shown by the open circles in the left panel of Fig. 8. The raw super-ratio is above the absolute limit of $T = 1$ because of the asymmetric Fresnel reflections in

the two measurements. For radiation at normal incidence, the fraction of light reflected at an interface is determined completely by the indices of refraction of the materials [22]

$$R(\lambda) = \frac{(n_1 - n_2)^2}{(n_1 + n_2)^2}. \tag{3}$$

In the case of the measurement as described above, the asymmetric interfaces are the C_6F_{14}/MgF_2 and the N_2/MgF_2 boundaries in the flow cell. A
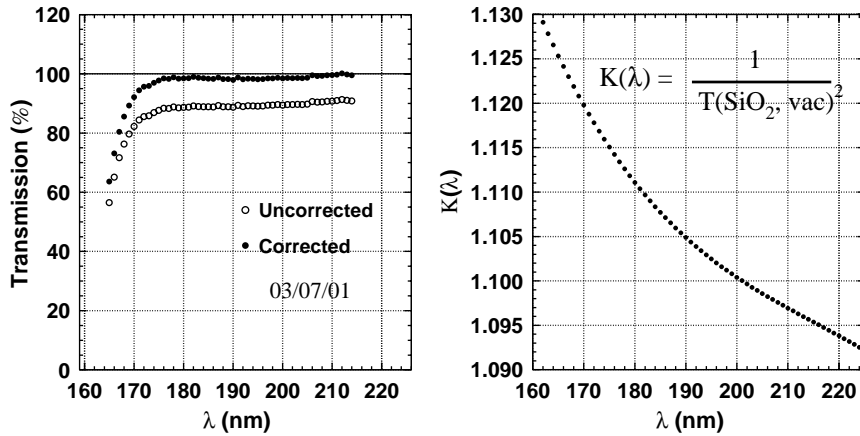
Fig. 9. The transmission for quartz before and after the correction for the Fresnel reflections is shown in the left panel. The correction factor κ which is applied to the super-ratio to determine the corrected transmission is shown in the right panel.

correction factor κ, must be applied to the super-ratio to determine the transmission

$$\kappa(\lambda) = \frac{(1 - R_1)^2}{(1 - R_2)^2} = \frac{(T_1)^2}{(T_2)^2}, \tag{4}$$

where R_1 and R_2 are the reflection coefficients at the N_2/MgF_2 and C_6F_{14}/MgF_2 interface, respectively, as determined by Eq. (3) and T_1 and T_2 are the corresponding transmitted fractions. The correction factor κ, is shown in the right panel of Fig. 8. The wavelength dependence of the corrected super-ratio is defined to be the transmission coefficient T, and is shown by the solid circles in left panel of Fig. 8. No other normalization is applied.

A transparency measurement has also been carried out on a 5 mm thick piece of quartz similar in specification to that used for the liquid containment vessels. The relative transmission curve along with the Fresnel correction is shown in Fig. 9.

The transmission coefficient can be converted to an absorption length (X_o) which is the thickness of material where the intensity of light falls to e^{-1}. It is related to the transmission coefficient T via

$$X_o = \frac{-1}{\ln(T)}, \tag{5}$$

where l is the sample thickness. The transmission coefficients and corresponding absorption lengths,

for a sample of clean and raw liquid, are shown in the left panel of Fig. 10, while a similar plot for the quartz sample is shown in the right panel.

5. Results

5.1. Liquid transparency

The transparency of the liquid after one month of cleaning, along with the transparency of the raw liquid, has already been shown in Fig. 10. The integrated transmission, $\int T$, is a useful quantity to compare different transmission spectra and is defined by Eq. (6):

$$\int T = \int_{\lambda_l}^{\lambda_u} \frac{dT}{d\lambda} d\lambda, \tag{6}$$

where the integral bounds are defined by the upper (λ_u) and lower (λ_l) wavelength and $dT/d\lambda$ is the wavelength dependent transmission of the liquid. Over the wavelength region of $160 < \lambda$ (nm) < 225 the integrated transmission is measured to be 45.6 ± 1.5 and 57.1 ± 0.5 for the raw and clean sample, respectively[6] which corresponds to 71.2% and 89.2% of the total. This implies the raw liquid transmits only 79.8% of the cleaned liquid. All

---

[6] For a perfectly transparent liquid, $\int T = \int_{\lambda=161\ nm}^{\lambda=225\ nm} (dT/d\lambda) d\lambda = 64$.
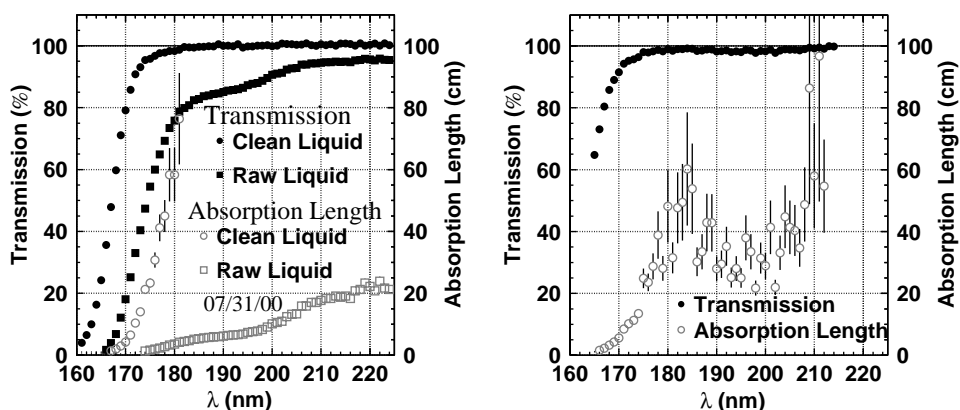
Fig. 10. The left panel shows the transmission of perfluorohexane after circulation in the liquid system for one month (solid circles) as well as the transmission of raw liquid, as obtained from the manufacturer (solid squares). The corresponding absorption lengths are shown by the open markers. The right panel shows the transmission and absorption lengths for the quartz sample.

other $\int T$ values will be quoted for this wavelength range unless stated otherwise.

5.1.1. Accuracy and precision

The transmission spectra discussed throughout this paper are measured at 1.0 nm intervals with a wavelength spread of approximately ± 0.10 nm for each point. In order to determine the photo-current at a specific wavelength, approximately 1200 individual measurements are made from which the mean is extracted. The resolution of the bi-alkali PMT anode current measurements, defined by the width over the mean, $(R = \sigma/\text{mean})$, for the wavelength region $190 < \lambda$ (nm) < 225 is 1.73% and 2.33% for the signal and reference tubes respectively. This is shown in the left panel of Fig. 11. The difference in the resolution between the two detectors can be attributed to variations in the reflectance over chopper blades,[7] as well as a lower spectral sensitivity of the reference PMT compared to the signal PMT. The error on the mean value of the anode currents is $\leqslant 4 \times 10^{-3}$ and the error on the ratio R_F and/or R_G is $\leqslant 6 \times 10^{-4}$. This propagates an uncertainty of $\leqslant 2 \times 10^{-3}$ to the uncorrected transmission coefficient or super-ratio

(i.e., $|\delta\mathscr{R}| \leqslant 0.002$). The error on the Fresnel correction factor κ, is dominated by the error on the index of refraction of the liquid. Measuring an index of refraction in the VUV region is difficult and little data exists for our particular case [23]. However an error can be estimated from the data. A distribution of the *corrected* transmission values in the wavelength interval $190 < \lambda$ (nm) < 225 is shown in the right panel of Fig. 11. In this region the liquid transparency is essentially constant with a mean transmission of 100.51% and a width (σ) of 0.36%. The error on κ can be estimated to lie between the limits of σ and the excess over 100% of the measured mean transparency (0.51%). Folding this with the error on the super-ratio gives a total error on the transmission measurement of $\delta T \leqslant 0.006$ or 0.6%.

The mean transmission value of the liquid being above 100% can be attributed to an incorrect value for κ. In order to produce a transmission value of 100% in the spectral range $190 < \lambda$ (nm) < 225, the value of κ must be decreased by ~ 0.0044. If this is solely attributable to an error in the value of the index of refraction of perfluorohexane,[8] the index of the liquid is too large by $\sim 2 \times 10^{-3}$. This is about a factor of 2

---

[7] Data for these plots were acquired by triggering on a specific single blade to reduce the variation in reflectivity as much as possible. See Section 4.1 for a description of the trigger.

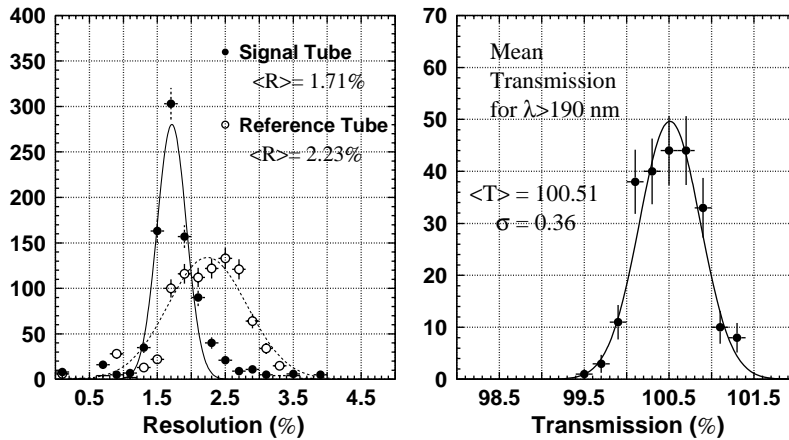[8] There is also an uncertainty in the index of MgF$_2$ but it is expected to be smaller.

Fig. 11. The resolutions of the current measurements made by the bi-alkali photo-tubes for the wavelength region above 190 nm are shown in the left panel. The spread in the corrected transmission for perfluorohexane in the wavelength region above 190 nm is shown in the right panel.
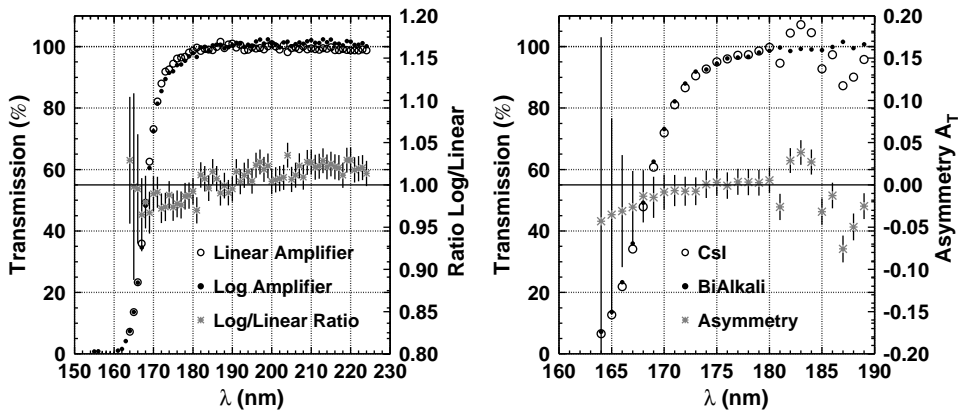

Fig. 12. A comparison between the C_6F_{14} transmission as measured with the logarithmic and linear current to voltage converters on the bi-alkali PMTs is shown in the left panel. A comparison between the transmission measured with the CsI and Bi-alkali PMTs is shown in the right panel.

larger than the temperature coefficient for the index of refraction of $5 \times 10^{-4}\,°C^{-1}$.

The systematic error can be estimated by comparing the results of transmission measurements between the different PMT tubes and the different amplifiers. The left panel of Fig. 12 shows two measurements made with the bi-alkali PMTs, one using the logarithmic and one using the linear amplifiers. The ratio between the two measurements is shown by the asterisks on the same plot. There is a systematic difference between the two where the logarithmic amplifier tends to measure a

smaller (larger) transmission at short (long) wavelengths with a maximum deviation of ± 0.030 ($\pm 3.0\%$). This discrepancy can be traced to the presence of a second order term in the transfer function of the logarithmic amplifier for currents smaller than 10 nA. The resolution of the current measurements with the bi-alkali PMTs and log amplifiers are 2.3% and 2.5% for the signal and reference tube, respectively. This is slightly larger than the values extracted from measurements with the linear amplifiers. The ratio of the integrated transmission for the linear

to log amplifiers in conjunction with the bi-alkali PMTs, is 1.000 ± 0.011 over the interval of $164 \leqslant \lambda$ (nm) < 225.

The right panel of Fig. 12 show a comparison between the bi-alkali and CsI PMTs with the same linear amplifiers. The region of comparison is limited to $\lambda \leqslant 180$ nm because of the small signal attributable to the rapidly falling QE of the CsI photo-cathode. The resolution of the measurements is 1.9% and 2.2% for the CsI signal and reference PMTs, respectively. It should be noted that these values are extracted from a different region than used for the bi-alkali tubes. The asymmetry between the measurements, as defined by

$$A_T = \frac{T_{\mathrm{CsI}} - T_{\mathrm{Bi-Alk}}}{T_{\mathrm{CsI}} + T_{\mathrm{Bi-Alk}}} \qquad (7)$$

is maximumly $4.3 \pm 21\%$ at 164 nm and decreases to $< 1\%$ for $\lambda \geqslant 170$ nm. The ratio of the integral transmission between the CsI PMTs and bi-alkali PMTs with the linear amplifiers over the wavelength region $164 \leqslant \lambda$ (nm) $\leqslant 180$ is 0.9984 ± 0.0014.

Comparing these measurement and the consistency between them, the systematic error on a single transmission measurement can be estimated to be the order of 0.5%, combining this with

the measurement error, gives a total error on a single transmission point of $|\delta T| = 0.0078$ or 0.78%.

5.2. Transparency evolution

In the summer 2000 RHIC run, a mixture of 20 l of liquid cleaned and utilized for the cosmic commissioning run from the previous year, and an additional 35 l of fluid pre-cleaned, as described in Section 3.2 was used in the recirculation system. At the start of the run, the 20 l of liquid was exposed to three molecular sieve changes over the period of two weeks. The pre-cleaned fluid (35 l) was then added with a simultaneous exchange of the sieve cartridge, and the system was then allowed to evolve over the course of nearly 2 months with no further intervention. The liquid transparency was measured periodically throughout this period to track the evolution as well as monitor the effectiveness of a single molecular sieve cartridge. The evolution of the transparency at several wavelengths, is shown in the left panel of Fig. 13. The time zero is the start-up of the liquid recirculation system when only 20 l liquid resided in the system (June 14, 2000). The dotted lines indicate points at which the filter cartridge was changed. This occurred at approximately 100 h
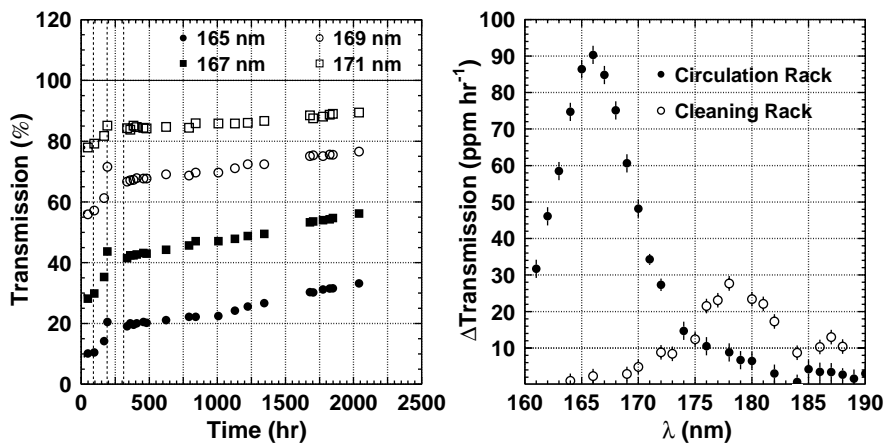

Fig. 13. The liquid transmission evolution over 2100 h is shown for four selected wavelengths in the left panel. The time spans from the system start-up to the end of the year 2000 RHIC run. The dotted lines indicate a filter cartridge change. On the right panel, the rate of change of the transparency versus wavelength is shown for the case of the circulation rack (solid circles) and the cleaning rack (open circles).

intervals for the first two weeks. The dotted line at ~ 300 h indicates the point at which the 35 l of pre-cleaned liquid was added to the system *and* the last filter change was made. All of the sieve exchanges, except the last, are accompanied by a jump in the measured transparency.

After the final intervention the transparency began to increase in a linear fashion throughout the remainder of the run. The rate of change in the transparency was extracted at each wavelength from this data and is shown by the solid markers in the right panel of Fig. 13. A similar analysis over 800 h was also done for the liquid circulating in the pre-cleaning system and results are shown by the open markers in the same figure. In the pre-cleaning rack, raw liquid is processed under a pressurized and stagnant atmosphere while in the recirculation system, clean and transparent liquid is further cleaned with the addition of a purging cover gas. As such the cleaning rack should initially have a larger increase in the transmission values at higher wavelengths. This will decrease once the transparency reaches values near 100%. When this condition is satisfied, further cleaning will have very little effect on this region.

In the pre-cleaning system the rate of change of the transmission is significantly smaller than in the circulation rack. The effectiveness is also shifted to larger wavelengths where the maximum change of 27.7 ppm h^{-1} occurs at 178 nm. For the recirculation system the maximal rate of change in the transparency of 90.3 ppm h^{-1} occurs at 166 nm. This corresponds to the maximum of the absorption cross-section of water (see Fig. 5). The rate of change of the transparency asymptotically approaches zero at larger wavelengths where the transmission is very near the 100% limit. The difference between the two racks indicates that the purging of the cover gas is an important component in the cleaning process. It also offers an explanation of why the transmission of the liquid dropped after the addition of the 35 l of liquid if the pre-cleaning procedure is not as efficient as the circulation rack.

If it is assumed that the change in transmission is solely due to the presence of water in the liquid, it is possible to extract the amount of water contained and removed from the liquid, given the absorption cross section as illustrated in Fig. 5. After the final filter exchange, (i.e. $t = 300$ h) the transmission at 166 nm was measured to be $29.4 \pm 0.3\%$. Given an absorption cross-section at this wavelength of 5.104 MB, the concentration of water is 4.3 ppm.[9] Over the course of the 2000 h, the transmission at 166 nm improved to $44.5 \pm 0.3\%$. If this increase is solely attributed to the removal of water, this corresponds to a decrease of water by 1.4 ppm in the liquid to 2.8 ppm. Given that the saturation content for water in the liquid is 10 ppm, this appears to be a fair estimate. However this relies on the assumption that there is no bathochromic shift in the water absorption spectrum in the presence of perfluorohexane. Furthermore, this does not take into account oxygen or other contaminants. Analysis of the liquid by gas chromatography provides evidence that the liquid may contain perfluoroheptane and/or perfluoroctane at the percent level [20]. More significant is that the presence of protons has also been ruled out at the $\geqslant 1$ ppm level by NMR measurements [21]. These results taken together point at oxygen as the prime contaminant in the system.

At the time of the initial fill of the recirculation system, in December 1999, a small amount (~ 250 ml) of raw liquid was dispensed from the shipment vessel into a glass Pyrex bottle with a plastic sealed top. The liquid was stored at normal room temperature under normal ambient conditions in the laboratory. This liquid was measured at the beginning of the 2000 RHIC run, 18 months after dispensing, and the transmission was found to have changed quite appreciably from the initial raw liquid. This is shown by the open circles in the left panel of Fig. 14. A strong absorption band at 185 nm and a weaker one at 205 nm becomes evident after long term exposure to the atmosphere. The transmission at 166 nm for this sample is $1.01 \pm 0.55\%$. Such attenuation would correspond to an unphysical concentration of ~ 25 ppm (by weight) of water. The asterisks show the transparency measured for the raw liquid as it is obtained from the manufacturer. The open

---

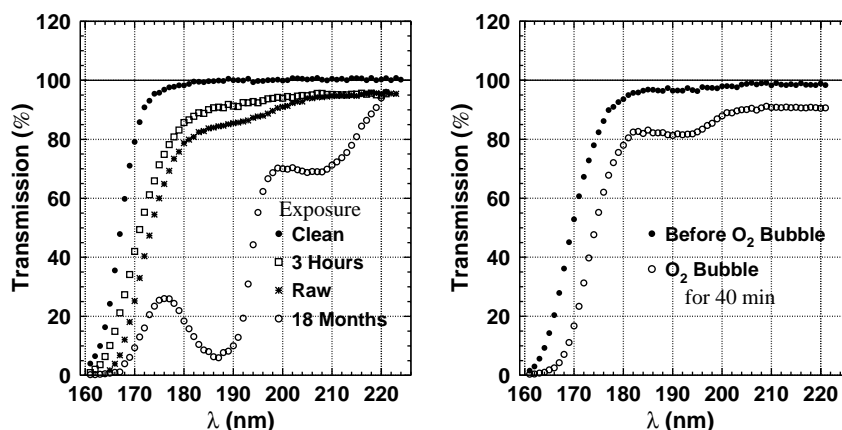[9] Water concentrations are specified as "ppm by weight" to ease comparison with Table 1.

Fig. 14. Transparency measurements of several C_6F_{14} samples. The left panel shows two control measurements of clean and raw liquid (also seen in Fig. 10) in addition to a clean sample exposed to the atmosphere for 3 h, and a sample of raw liquid after exposure to the atmosphere for 18 months. The right panel shows a sample extracted from the recirculation rack, and the same sample after exposure to an oxygen bubbler for 40 min.

squares show a measurement of a liquid sample that was extracted from the recirculation system and stored in a Pyrex bottle for 3 h before the measurement. In the wavelength region above $\lambda > 200$ nm, it is essentially identical to the raw liquid.

In order to determine whether the absorption was due to dissolved oxygen, a 100 ml sample of liquid was decanted from a used molecular sieve cartridge into a graduated cylinder. The transmission of this sample is shown by the solid circles in the right panel of Fig. 14 and gives an integrated transmission of 50.3 ± 0.6. Note that its transmission characteristics are between that of the clean liquid ($\int T = 57.1 \pm 0.5$) and the liquid exposed to the atmosphere for three hours ($\int T = 49.7 \pm 0.5$). Oxygen was then bubbled through the sample via a porous stone at a rate of several hundred ml h^{-1} for 40 min and the transparency remeasured. The results are shown by the open circles in the same panel. The integrated transmission is calculated to be 41.5 ± 0.6. The pronounced dip at ~ 190 nm, as observed in the raw liquid and the sample aged for 18 months, is also visible. It appears that the sample which had oxygen bubbled through it possesses the same systematic and qualitative features as samples which have been exposed to the atmosphere. Taken at face value it seems oxygen can account for the spectral features of the attenuation of the VUV transmission.

The presence of oxygen also seems to fit qualitatively with the behavior of the installation of a new regenerated molecular sieve. As mentioned in Section 3.1, the sieve cartridge gets warm when initially exposed to the liquid. The installation of a new sieve is also correlated with a discontinuous increase in the transparency of the liquid, both in the cleaning rack and the recirculation system. One could imagine that the local heating of the liquid liberates gases, including oxygen, from the liquid, and it is this mechanism which is responsible for the jump in transmission. This is being studied by measuring the temperature dependence of the liquid transparency.

If it is assumed that the longer the sample is exposed to the atmosphere (or oxygen) the larger the dissolved oxygen content, it would explain an increased attenuation of VUV radiation with age. However, it does not explain why the absorption band at ~ 190 nm seems to bathochromically shift with increased exposure length, unless it is a concentration dependent effect. The energy of this band is approximately 6.6 eV which corresponds to the energy of an $n \rightarrow \sigma^*$ excitation of the atomic electrons which could occur in either fluorine or oxygen. The fact that the absorption characteristics do not seem to follow the profile of the oxygen photo-absorption cross-section (see Fig. 5) hints that the photo-chemistry of the underlying

processes may be quite complex. If the naive assumption is made that the attenuation of the VUV radiation is due to *molecular oxygen*, then the O_2 concentration for the sample exposed to the atmosphere for 3 h (open squares in Fig. 10) can be deduced. At 190 nm, the transmission is 91.3% and the average absorption cross-section due to the SR bands is $\sim 10^{-20} cm^2$ (10 kB). This implies an oxygen content of $\sim 34 \pm 3$ ml/100 ml of liquid.[10] Using the same assumptions the raw liquid (asterisks in Fig. 10) would have an oxygen concentration of $\sim 60 \pm 3$ ml/100 ml. This is very close to the saturation content of O_2 in C_6F_{14} of 65 ml/100 ml. So it very well may be that the liquid quickly saturates with O_2 upon exposure to the atmosphere and there are slower chemical processes which alter the electronic structure of the liquid. This picture is further complicated by the measurement, since radiation below 242 nm (5.1 eV) can dissociate O_2, so $O^- - C_6F_{14}$, $O_2 - C_6F_{14}$, and even $O_3 - C_6F_{14}$ complexes may form which modify the electronic structure of C_6F_{14} and subsequent VUV absorption spectrum. This is a subject of a current investigation.

5.3. Stagnant tests

The transparency measurements described thus far are made with the liquid flowing through the MgF_2 sample cell at a rate of 4 l h^{-1}. However, the liquid is more or less stagnant in the radiator vessels of the detector for several hours. In fact the flow through the 5 l radiator vessels is 3 l h^{-1}. This raises the question of whether atomic interactions between the liquid and radiator vessel can affect the liquid transparency during extended stagnant periods. In the case of the spectrometer and the use of a MgF_2 windowed flow cell, it is possible that the unpaired electrons in the fluorine interact with the electrons in the perfluorohexane chain. This effect should be much stronger with MgF_2 than with quartz because the atomic structure is more similar. The effect of stagnant liquid can be tested by measuring the transparency of the liquid as a

function of time the liquid stands stagnant in the cell.

The relative transparency of the liquid as a function of time it remains stagnant in the cell is shown in Fig. 15. The logarithmic time scale extends from 1 min to 50 h. These measurements were made over a time period of approximately 350 h, with the shortest intervals being the last completed. The solid markers indicate the relative transparency of each measurement and this appears to decrease slightly. In view of the transparency evolution as described in Section 5.2, the transparency values must be corrected to remove this effect since the transparency at 166 nm changes by $|\delta T| = 0.025$ (i.e. $|\Delta T| = 2.5\%$) over this period.

The open markers illustrate the transmission at four separate wavelengths after the application of the transmission evolution correction. These data indicate that the transparency does not degrade when the liquid is allowed to stand stagnant over a time scale up to 50 h. This has several implications. First the transparency measurements carried out do not depend upon the time that the liquid is held stagnant in the cell. This means that the
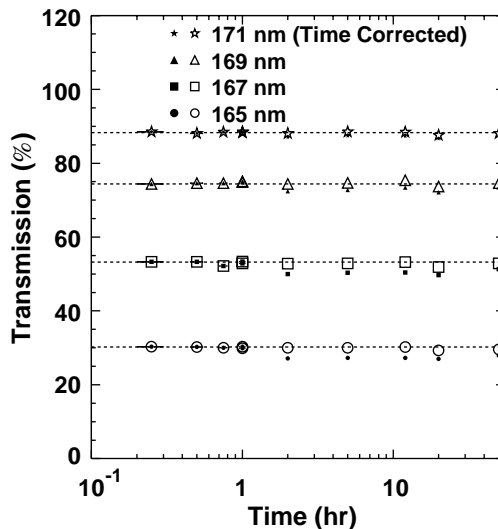

Fig. 15. Effect of the time the liquid stagnates in the sample cell on the measured transmission. The solid markers are the transparency measurements while the open markers are the transmission coefficients corrected for the 350 h time span of the measurements.

---

[10] Note that for the sample bubbled with O_2 has a transmission at 190 nm of 81.3% which corresponds to a O_2 content of 77 ml/100 ml.

transmission measured from the flowing liquid should be consistent with the liquid standing in the radiator vessels.

6. Conclusions

A liquid recirculation system is utilized to clean and distribute liquid to the radiator vessels of the STAR-RICH. This system performed safely and reliably over the first year run at RHIC. A VUV spectrometer, connected to the recirculation system, has been used to monitor the VUV transmission properties of the perfluorohexane liquid radiator used in the STAR-RICH detector. The device is a useful and flexible instrument which allows the measurement of transmission spectra over a large wavelength range. It is built in a modular fashion that allows exchange of components such as the photo-detectors, light source, and sample cell. This flexibility allows investigation of solid, liquid, as well as gas samples. By using a series of ratio measurements the transparency of samples can be measured with little dependence on the absolute calibration of the device components. Furthermore there is very little uncertainty introduced by systematic or time dependent effects. The accuracy and precision of the measurements extracted from comparisons of transparency measurements made with different electronics and PMTs are estimated to be 0.008 ($|\Delta T| = 0.8\%$).

In terms of the liquid transparency for the RICH detector, a very simple and conservative cleaning approach has been employed for the first year of detector operations. A molecular sieve cartridge has been used to remove water from the system while a continually flushed nitrogen cover gas isolates the perfluorohexane from the atmosphere and exhausts contaminants which out-gas from the liquid. The transmission measurements over the course of the run suggest that even without numerous exchanges of filter cartridges, the liquid transparency systematically improves. This implies that the liquid transparency is not compromised by the extended use of a molecular sieve over a period of at least two months in this application. The comparison between the cleaning rates of the cleaning and recirculation systems imply that oxygen is an important contaminant to consider and the N_2 purge of the cover gas is an important component of the liquid purification. These results have led to modifications of the gas purification for the liquid recirculation system such as addition of Oxisorb filtration cartridges as well as a $CaCO_3$ desiccant on the input nitrogen. The strategy to clean the liquid for the upcoming run is to initially change the molecular sieves quickly and often, on the time scale of days, and then let the system evolve without further intervention.

Acknowledgements

References

[1] A detector for high momentum PID, ALICE Technical Design Report, CERN/LHCC 98-19, 1998.

[2] The Compass Collaboration, Common Muon and Proton Apparatus for Structure and Spectroscopy, CERN/SPSLC/96-14, March 1, 1996.

[3] K. Zeitelhack, et al., Nucl. Instr. and Meth. A 433 (1999) 235.

[4] F. Piuz, Nucl. Instr. and Meth. A 371 (1996) 96; F. Piuz, et al., Nucl. Instr. and Meth. A 433 (1999) 178.

[5] The STAR-RICH Collaboration, Proposal for a ring imaging Cherenkov detector in STAR, YRHI 98-22, September 28, 1998.

[6] A. Di Mauro, Nucl. Instr. and Meth. A 433 (1999) 190; other samples and measurements vary considerably. For example see; G. Malamud, et al., Nucl. Instr. and Meth. A 343 (1994) 121; J. Seguinot, et al., Nucl. Instr. and Meth. A 297 (1990) 133; H. Rabus, et al., Nucl. Instr. and Meth. A 438 (1999) 94.

[7] G. Belanger, P. Sauvageau, C. Sandorfy, Chem. Phys. Lett. 3 (1969) 649.

[8] W. Adam, et al., Nucl. Instr. and Meth. A 343 (1994) 68;
D. Leith, Nucl. Instr. and Meth. A 265 (1988) 120.

[9] 3M Chemicals; 3M Center, St. Paul MN, 55144-1000.
http://www.3M.com.

[10] Uetikon 13X-1001; ZeoChem, PO Box 35940, Louisville
KY, 40232. http://www.zeochem.com

[11] Ultra-filter Inc, 3560 Engineering Dr, Norcross GA, 30092
http://www.ultrafilter.com

[12] G. Lenzen, et al., Nucl. Instr. and Meth. A 343 (1994) 268.

[13] J.M. Dalin CERN EST/SM Group. STAR-RICH Internal
Report, June 15, 1999.

[14] Oxisorb from Messer Griesheim, 3 Great Valley Pkwy,
Malvern PA, 19355. http:///www.mgindustries.com

[15] See G. Lenzen, Nucl. Instr. and Meth. A 343 (1994) 268.
and references therein.

[16] A. Di Mauro, et al., Nucl. Instr. and Meth. A 433 (1999)
190.

[17] S. Ogawa, M. Ogawa, Can. J. Phys. 53 (1975) 1845;
K. Watanabe, M. Zelikoff, Opt. Soc. Am. 43 (9) (1953) 753
and from the Harvard-Smithsonian Center for Astrophysics see http://cfa-www.harvard.edu/amdata/ampdata/
newcfamols.shtml.

[18] K. Yoshino, et al., J. Phys. Chem. Ref. Data 13 (1984)
207.

[19] K. Dickinson, W.C. Johnson Jr., Appl. Opt. 10 (1971)
681.

[20] B. Lasiuk, N. Baker, Analysis of Perfluorohexane YRHI-
01-33, March, 2001.

[21] B. Lasiuk, Spectroscopic Characterization of Perfluoro-
hexane, in preparation.

[22] J.D. Jackson, Classical Electrodynamics, Wiley, New
York, 1998.

[23] P.G. Moyssides, S. Maltezos, E. Fokitis, J. Mod. Opt. 47
(2000) 1693.